Supporting Information

Improving Cycling Stability and Rate Performance of Aqueous Sodium-Ion Supercapattery via Mitigating Metal Dissolution and Boosting Conductivity by Anchoring FePBA on rGO

Sheetal Gupta[a], *Mayank K. Singh*[a], *Sarathkumar Krishnan*[a], *Suporna Bhowmik*[a], *Khushwant Singh*[a], *and Dhirendra K. Rai*[a]*

[a]Sustainable Energy & Environmental Materials (SEEM) Lab, Department of Metallurgical Engineering and Materials Science (MEMS), Indian Institute of Technology Indore, Simrol, Khandwa Road, Indore 453552, India.

*Corresponding author: *Tel: +91 731 660 3278*

E-mail: dkrai@iiti.ac.in (D K Rai)

List of Content

Table S3. Calculated resistance and diffusion coefficient from EIS spectra of FPBA and FPBA/rGO composite.

Fig. S11. Bode phase angle plots for rGO, FPBA, and FPBA/rGO composite**.**

Fig. S12. Cyclic stability of FPBA and FPBA/rGO composite at 10 A g^{-1} for 10000 cycles.

Fig. S13. PXRD data of FPBA/rGO fresh and after 1000 cycles.

Fig. S14. (a-b) FESEM and EDX spectra of (a) FPBA electrode fresh and (b) FPBA electrode after 1000 cycles, (c) Iron atomic ratio % comparison between fresh and after 1000 cycles FPBA electrode, (d-e) FESEM and EDX spectra of (a) FPBA/rGO composite electrode fresh and (b) FPBA/rGO composite electrode after 1000 cycles, (f) Iron atomic ratio % comparison between fresh and after 1000 cycles FPBA/rGO composite.

Table S4. The concentration of $[Fe(CN)_6]^{4-}$ and $[Fe(CN)_6]^{3-}$ before and after 1000 cycles was calculated according to the UV-Vis spectra.

Fig. S15. (a) CV profile of the SScD at scan rates from 10 mV s^{-1} to 100 mV s^{-1}; (b) GCD profiles of the SScD at current densities from 1 A g^{-1} to 10 A g^{-1} (c) Specific capacity of SScD Vs. current densities (1-10 A g^{-1}) plot for FPBA SScD.

Fig. S16. Kinetics calculation based on the frequency ($\omega^{-1/2}$) and Z' values of fresh and after 10000 cycles of the FPBA/rGO composite SScD**.**

Table S5. Calculated resistance and diffusion coefficient from EIS spectra of fresh and after 10000 cycles of the FPBA/rGO composite SScD.

Table S6. Comparison table of FPBA/rGO composite SScD.

S1. Synthesis of GO and rGO

To synthesize graphene oxide (GO), 4 gm of graphite flakes and 2 g of $NaNO_3$ were added to 140 mL of H_2SO_4 in a 500 mL flask while stirring in an ice bath. Afterward, 12 g of $KMnO_4$ was gradually added, keeping the temperature at 20°C. Subsequently, the ice bath was removed, and the reaction mixture was heated to 50°C and stirred for 18 h. Then it was cooled to room temperature, and 220 mL of deionized water and 10 mL of H_2O_2 were added and further stirred for 4 h. Finally, the reaction mixture was filtered, and the product was washed with 10% HCl, DI water, and ethanol, and then dried in a vacuum oven to obtain GO. To obtain rGO, 500 mg of GO was dispersed in 80 mL of water through sonication and then stirred for 1 h. Afterward, 7 mL of hydrazine hydrate was added at 20°C, and then the reaction mixture was heated to 100°C for 25 h. Finally, the reaction mixture was washed with DI water and ethanol and dried in a vacuum oven to get the dry powder of rGO.

Table S1. Rietveld refined parameters for $Na_{2-x}FeFe(CN)_6$ sample.

Cubic (Fm-3m); a=b=c=10.33(Å); α=β=γ= 90°; V=1102.30 Å^3; R_{wp} =3.99%, Chi^2 =3.2					
Atoms	Wyckoff	x	y	z	Occupancy
Na	8c	0.25000	0.25000	0.25000	0.750
Fe1	4a	0.00000	0.00000	0.00000	1.000
Fe2	4b	0.50000	0.50000	0.50000	1.000
C	24e	0.25000	0.00000	0.00000	1.000
N	24e	0.50000	0.00000	0.00000	1.000

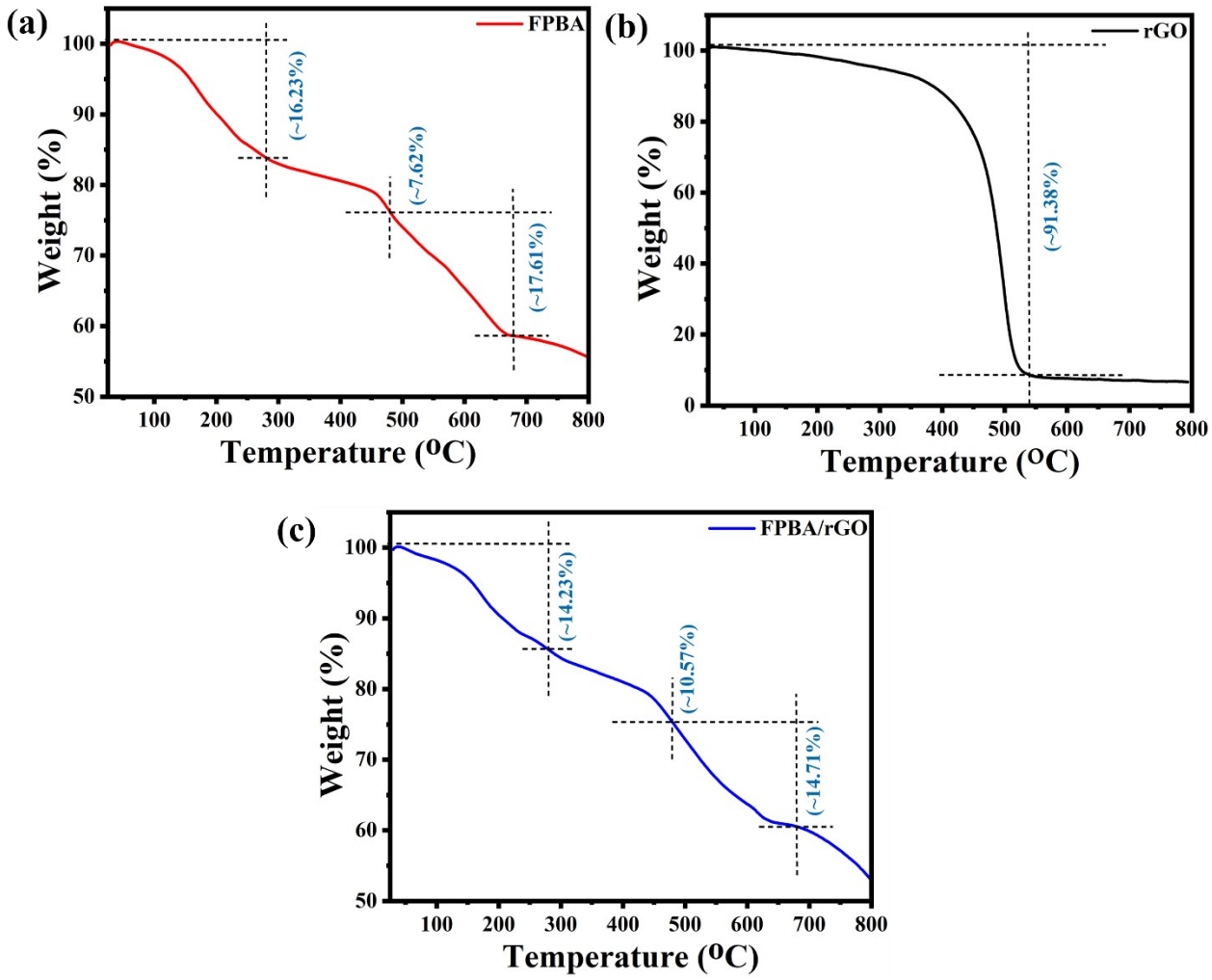

Fig. S1. TGA profile of (a) FPBA, (b) rGO, and (c) FPBA/rGO composite.

Table S2. Comparison of **FPBA**, **rGO**, and **FPBA/rGO** composite weight loss percentage**.**

Sample	**Weight loss in %**		
	1	**2**	**3**
FPBA	16.23 % (30-280˚C)	7.62 % (280-480˚C)	17.61 % (480-680˚C)
rGO	91.38 % (30-540˚C)		-
FPBA-rGO	14.23 % (30-280˚C)	10.57 % (280-480˚C)	14.71 % (480-680˚C)

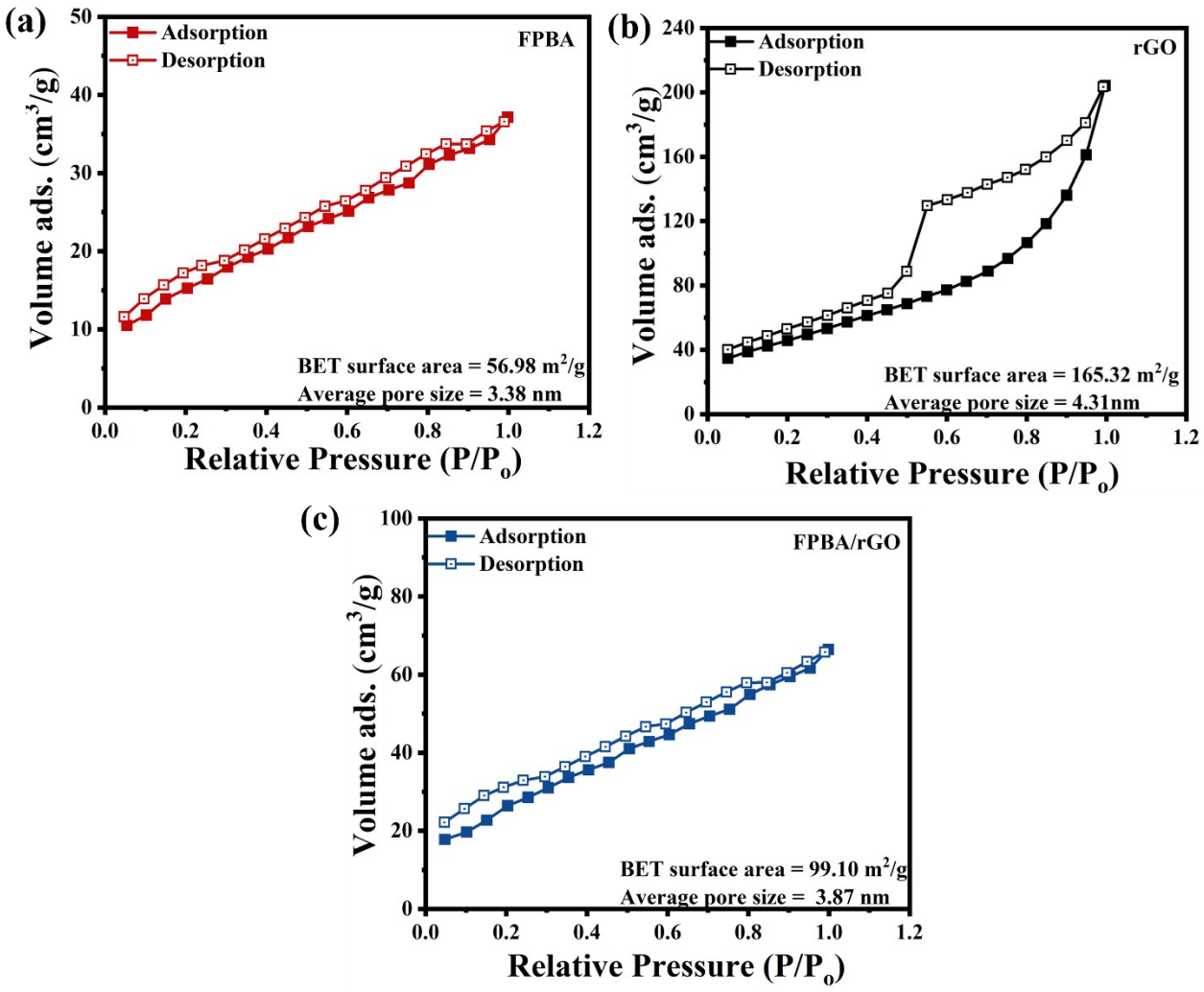

Fig. S2. N_2 adsorption-desorption isotherm of (a) FPBA (b) rGO, and (c) FPBA/rGO composite.

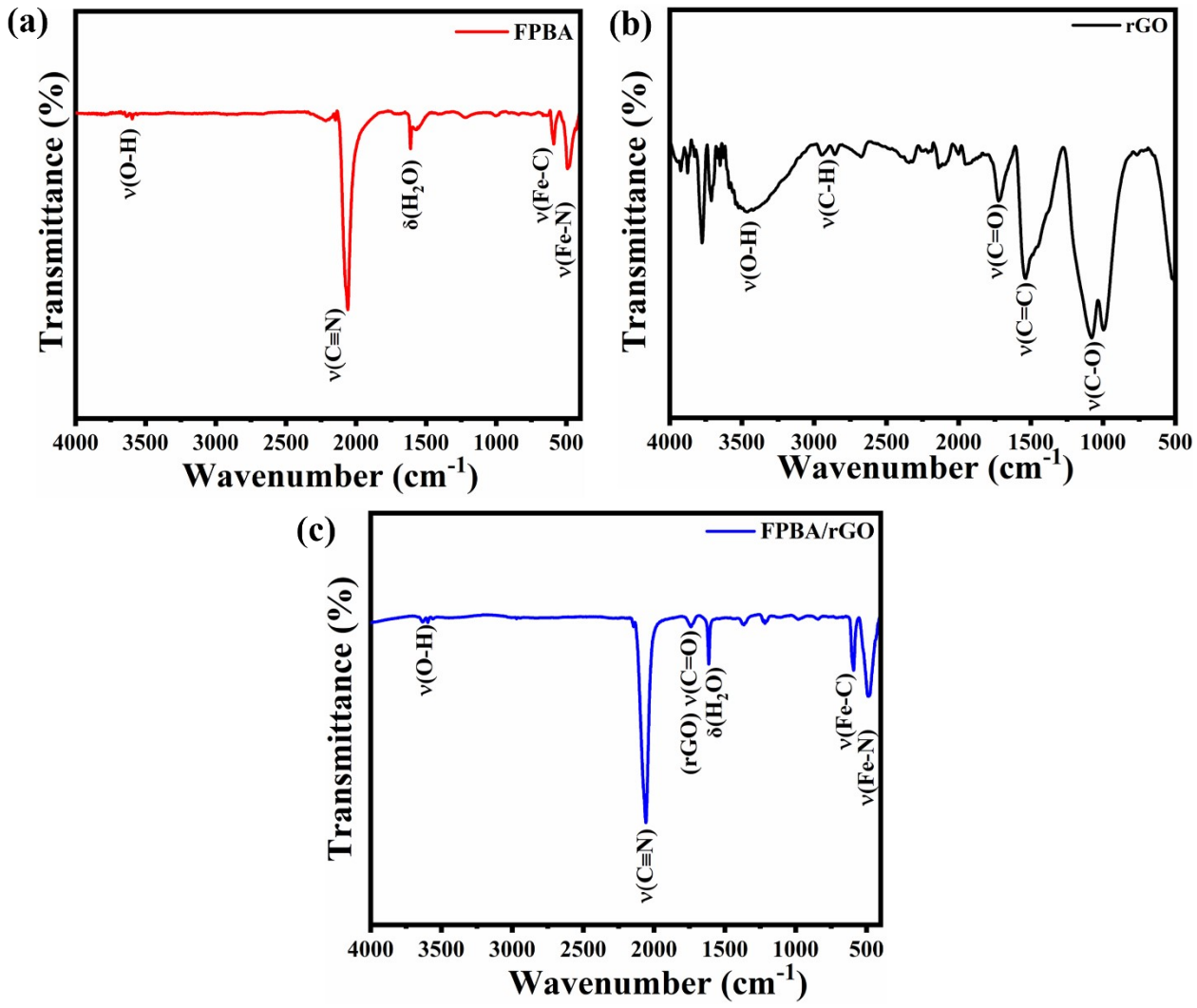

Fig. S3. FTIR spectra of (a) FPBA, (b) rGO, and (c) FPBA/rGO composite**.**

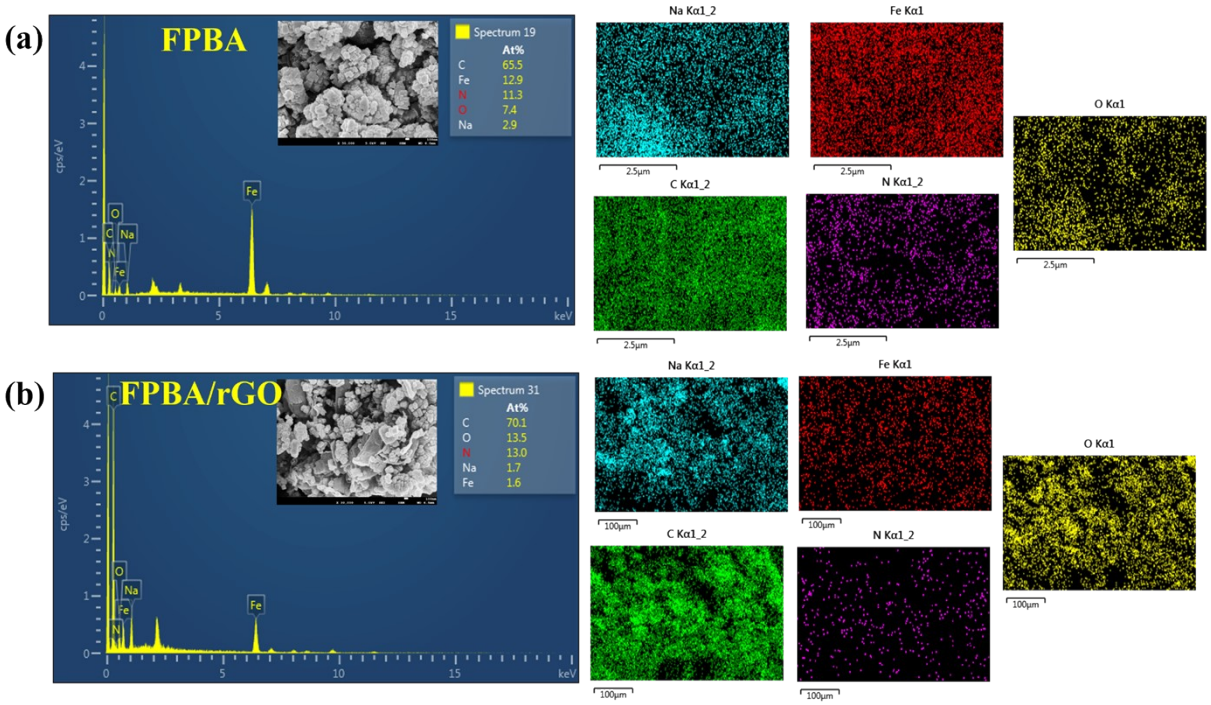

Fig. S4. EDX spectra and mapping of Na, Fe, C, N, and O elements in FPBA and FPBA/rGO composite**.**

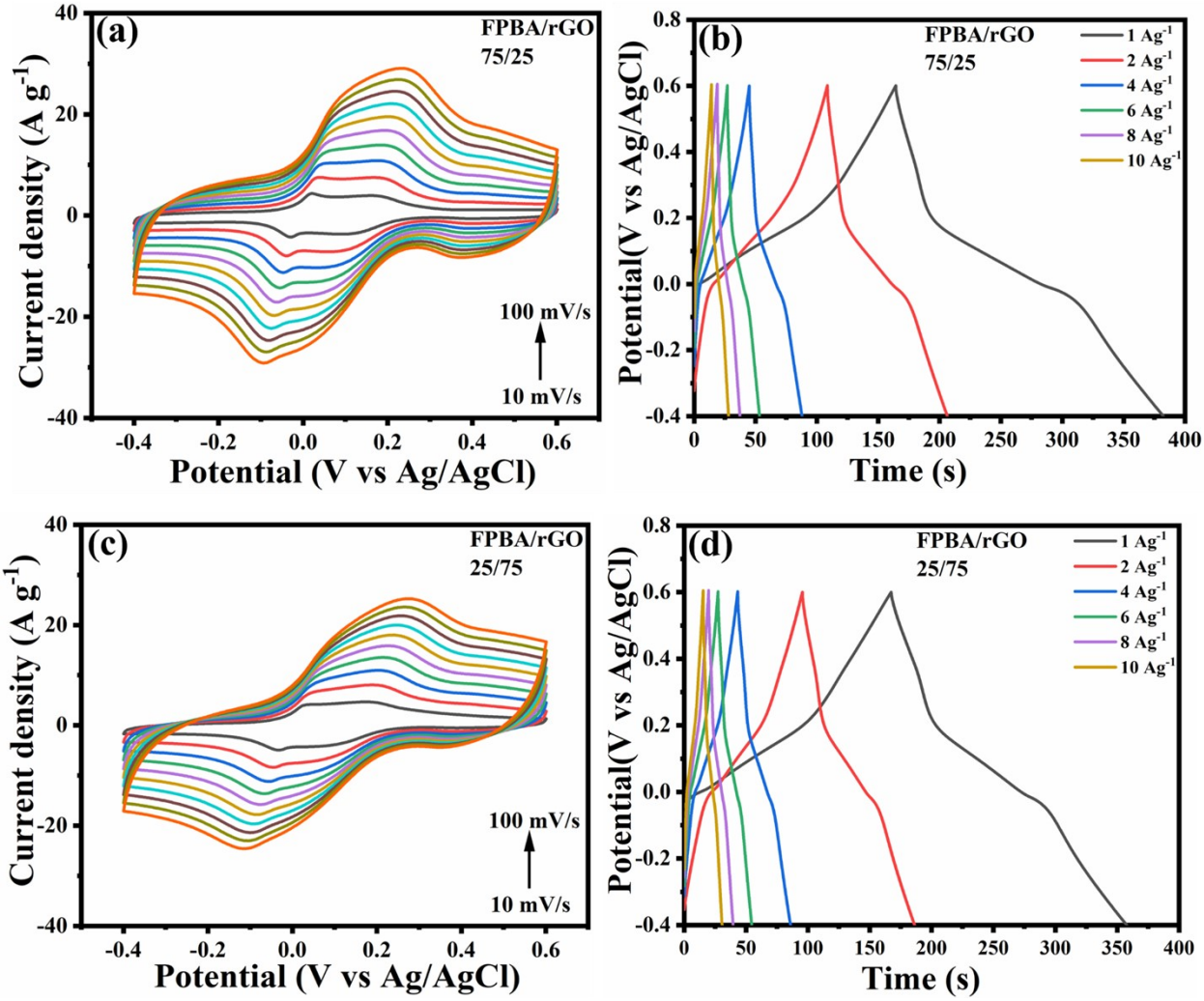

Fig. S5. (**a-d**) CV and GCD profiles of FPBA/rGO composites with different ratios of FPBA and rGO at varying scan rates and current densities.

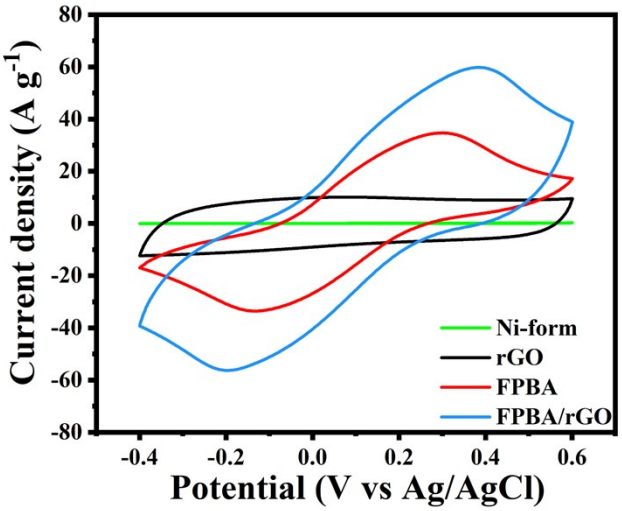

Fig. S6. CV profile comparison of bare Ni-form, rGO, FPBA, and FPBA/rGO composite at 100 $mV.s^{-1}$ scan rate.

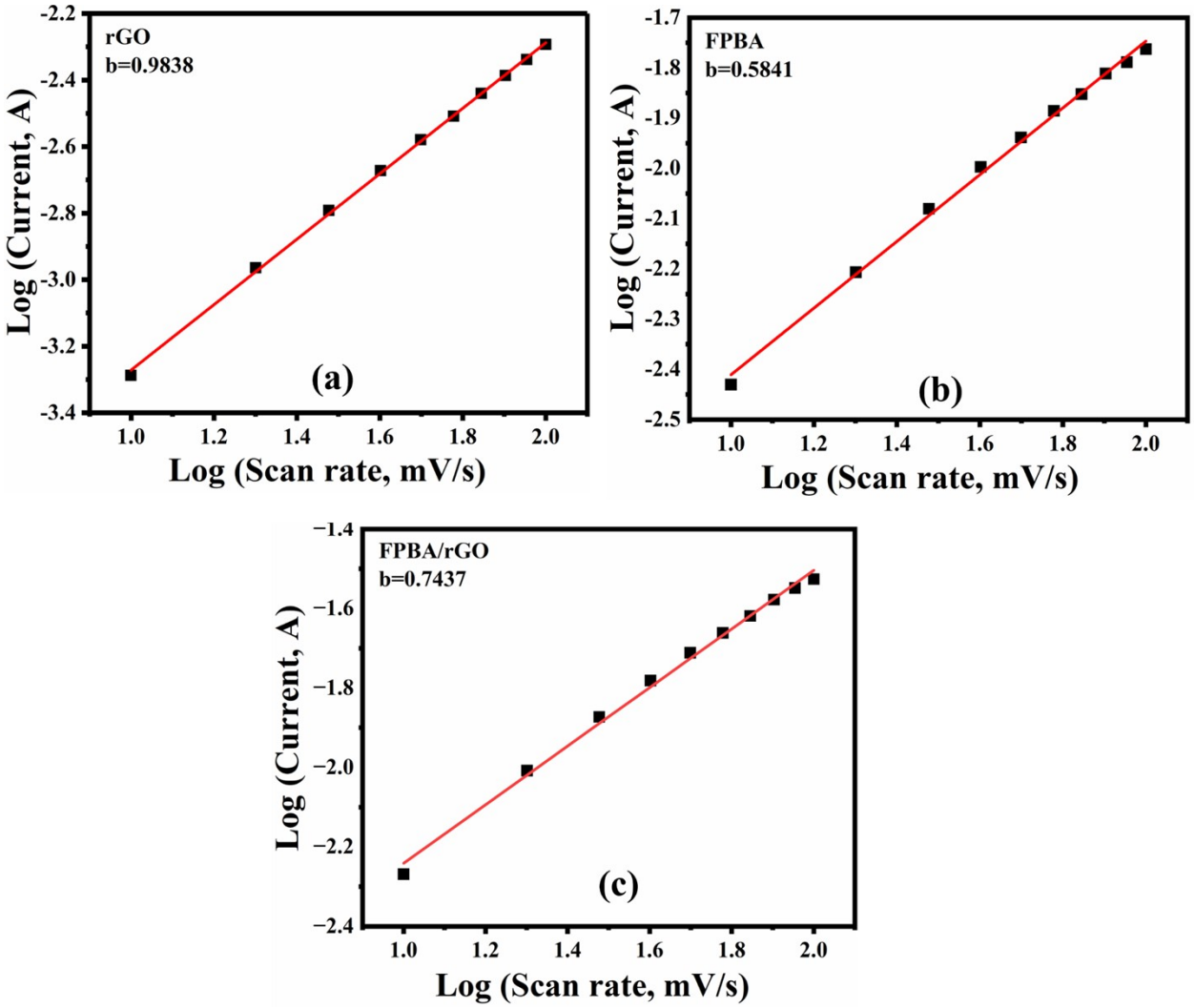

Fig. S7. Charge storage kinetics log (highest current, A) vs. log (scan rate, mV s^{-1}) graph plots of (a) rGO, (b) FPBA, and (c) FPBA/rGO composite.

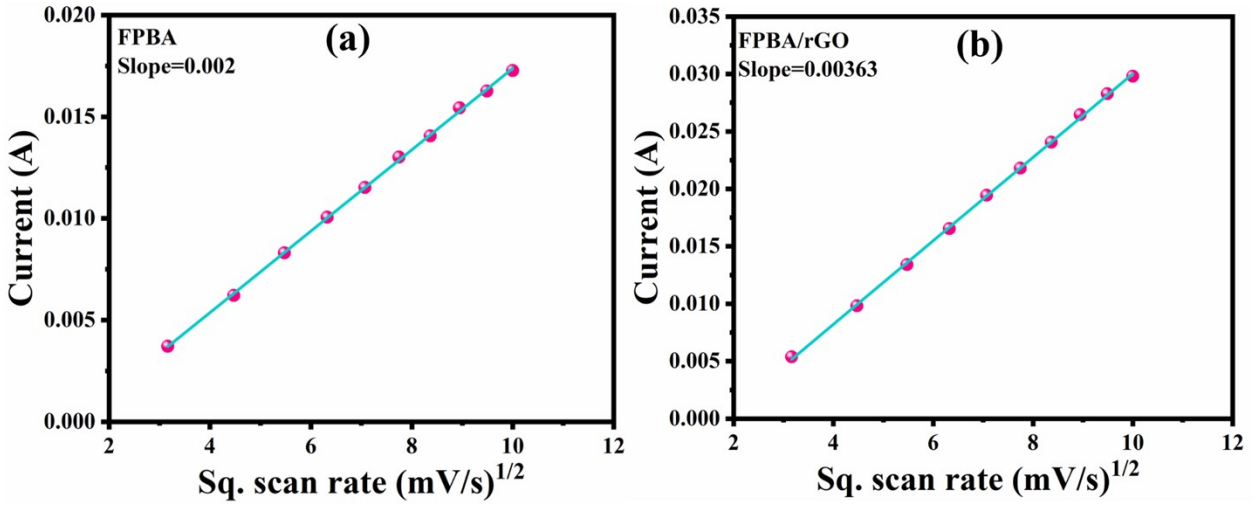

Fig. S8. Electrochemical kinetics analysis: Peak current (highest current, A) vs. square root of scan rate $(mV\ s^{-1})^{1/2}$ graph plots of (a) FPBA, and (b) FPBA/rGO composite at different scan rates between 10 to 100 mV s^{-1}. It is observed that the peak currents for both electrodes exhibit a linear relationship with the square root of the scan rate.

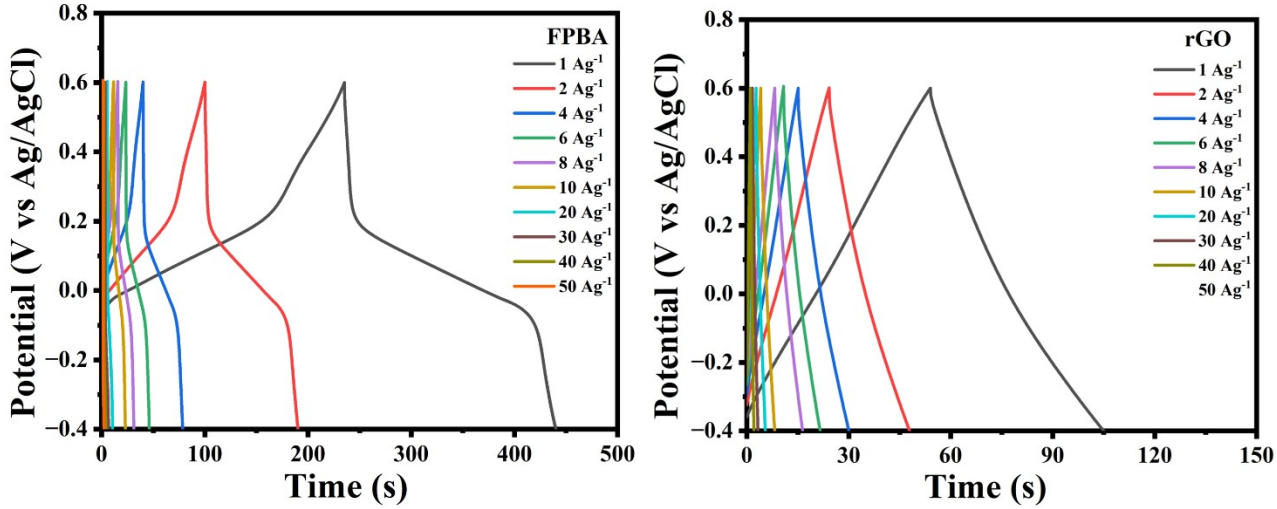

Fig. S9. GCD profile comparison of (a) FPBA and (b) rGO at various current densities ranging from 1-50 A g^{-1}.

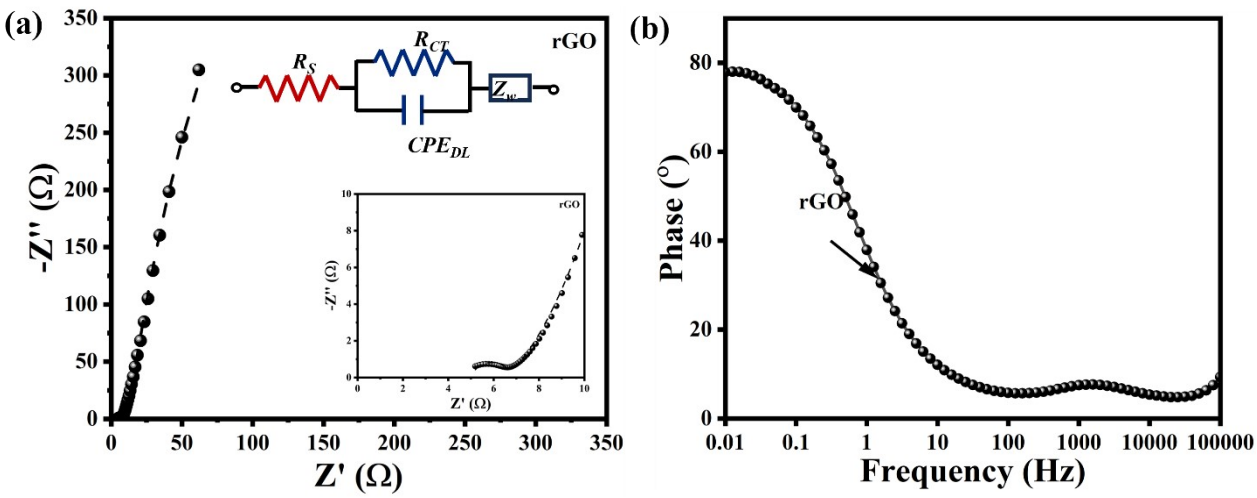

Fig. S10. (a) Nyquist plot and equivalent Randles circuit, (b) Bode phase angle plots of rGO.

Table S3. Calculated resistance and diffusion coefficient from EIS spectra of FPBA, FPBA/rGO composite and rGO.

	R_S (Ω)	R_{CT} (Ω)	σ (Ω $s^{-1/2}$) (from *EIS Fitting)*	σ (Ω $s^{-1/2}$) (from Randles circuit)	D_{Na+} (cm^2 s^{-1})
FPBA	4.454	3.501	7.602	7.013	3.881×10^{-11}
FPBA/rGO	4.19	2.431	4.180	3.936	1.283×10^{-10}
rGO	5.033	1.445	39.35	-	-

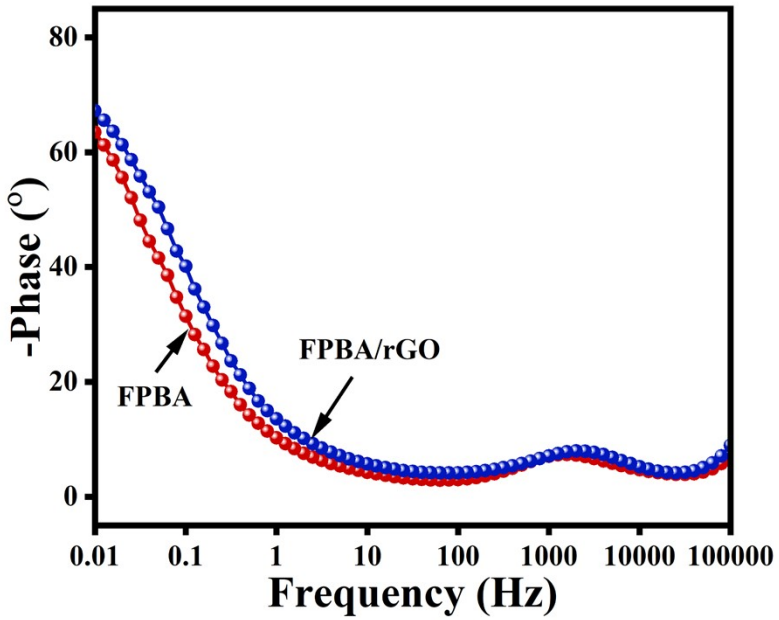

Fig. S11. Bode phase angle plots of FPBA and FPBA/rGO composite

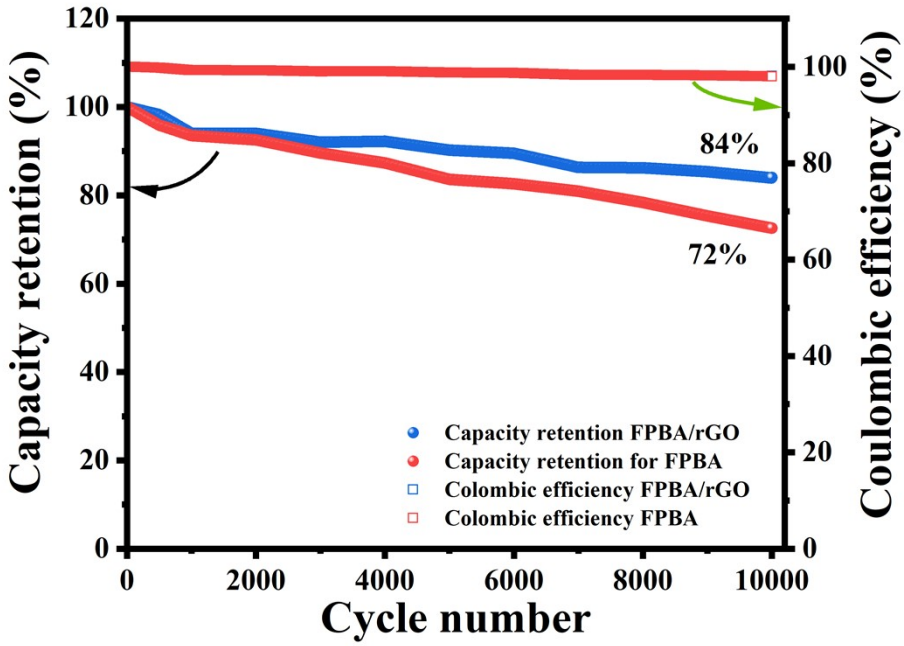

Fig. S12. Cyclic stability of FPBA and FPBA/rGO composite at 10 A g^{-1} for 10000 cycles.

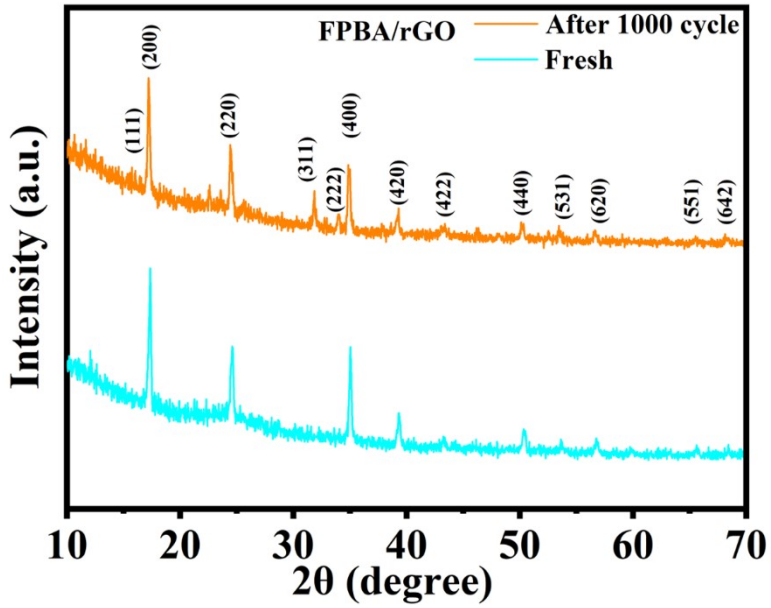

Fig. S13. PXRD data of FPBA/rGO fresh and after 1000 cycles.

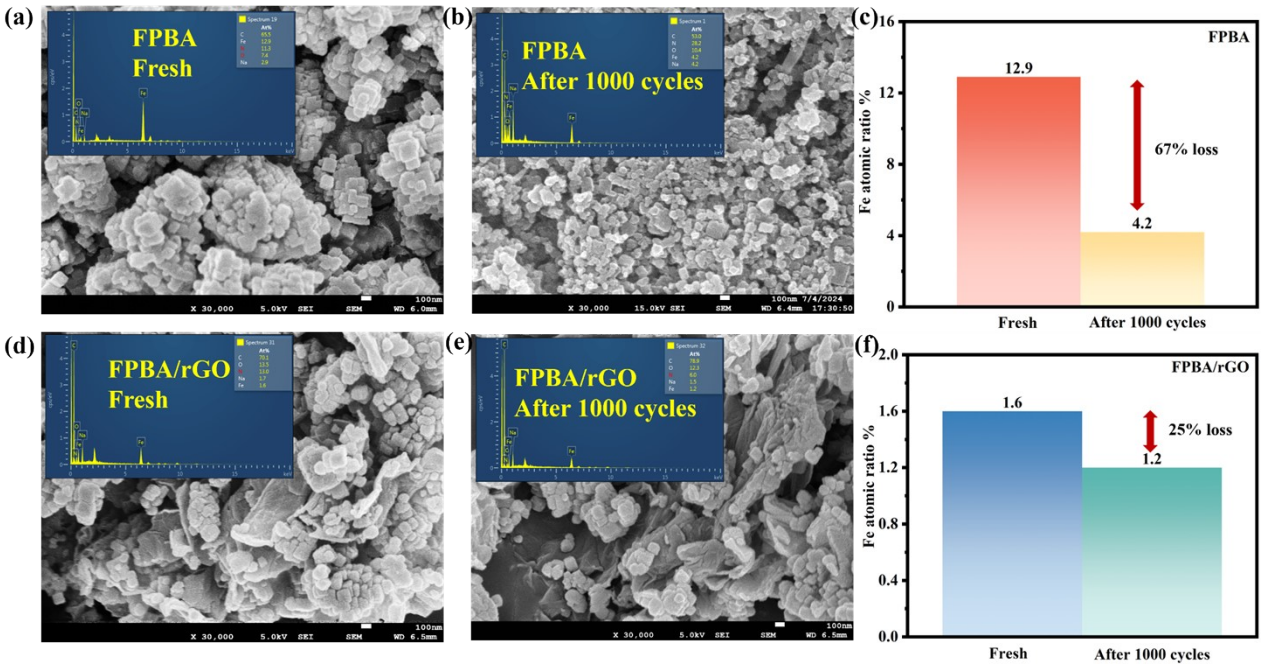

Fig. S14. (a-b) FESEM and EDX spectra of (a) FPBA electrode fresh and (b) FPBA electrode after 1000 cycles; (c) Iron atomic ratio % comparison between fresh and after 1000 cycles FPBA electrode; (d-e) FESEM and EDX spectra of (d) FPBA/rGO composite electrode fresh and (e)

FPBA/rGO composite electrode after 1000 cycles; (f) Iron atomic ratio % comparison between fresh and after 1000 cycles FPBA/rGO composite.

Table S4. The concentration of $[Fe(CN)_6]^{4-}$ and $[Fe(CN)_6]^{3-}$ after 1000 cycles was calculated according to the UV-Vis spectra.

Concentration	**$[Fe(CN)_6]^{4-}$ (mM)**	**$[Fe(CN)_6]^{3-}$ (mM)**	**Total (mM)**
FPBA after 1000 cycles	0.328	0.208	0.536
FPBA/rGO after 1000 cycles	0.15	0.045	0.195

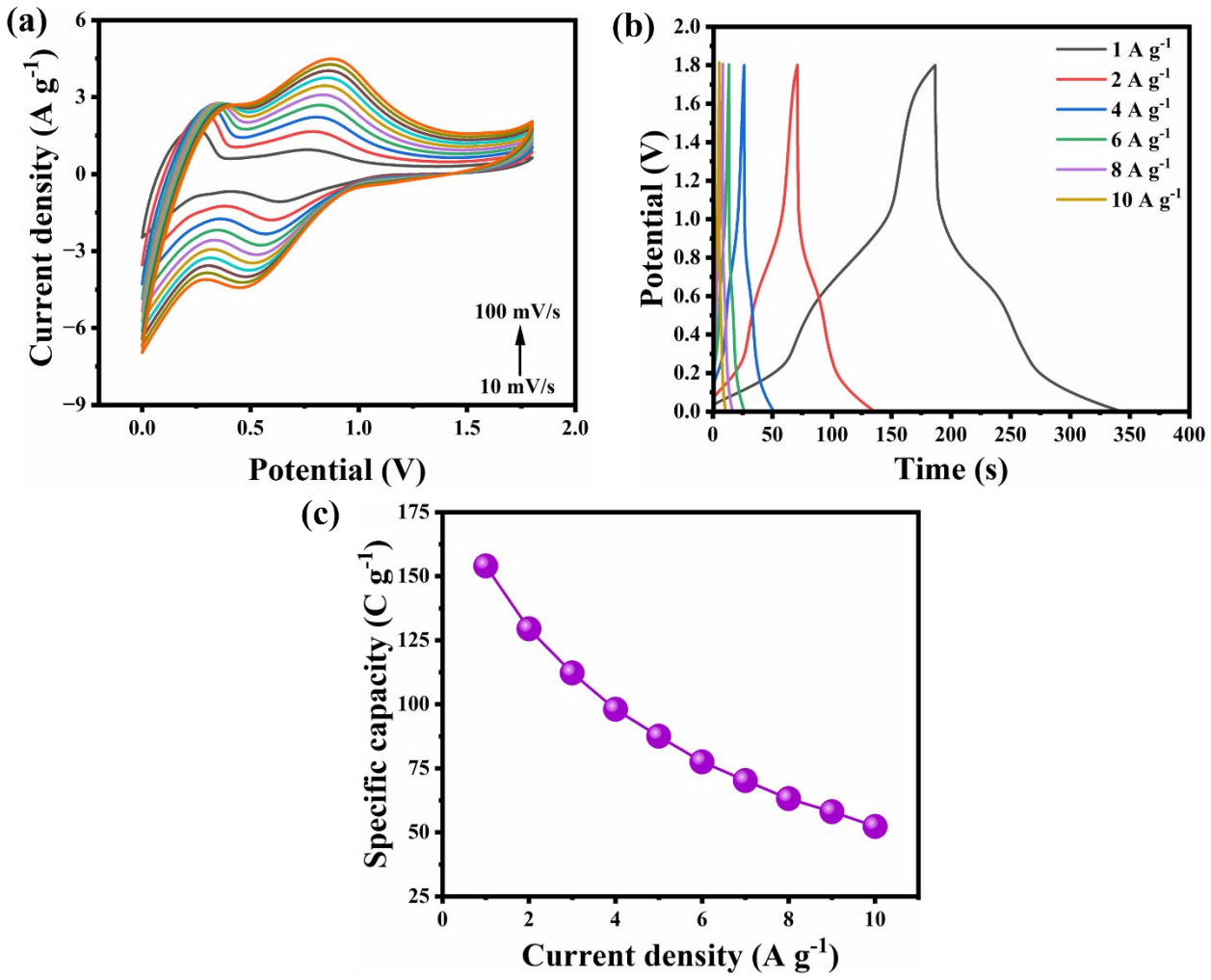

Fig. S15. (a) CV profile of the SScD at scan rates from 10 mV s^{-1} to 100 mV s^{-1}; (b) GCD profiles of the SScD at current densities from 1 A g^{-1} to 10 A g^{-1} (c) Specific capacity of SScD Vs. current densities (1-10 A g^{-1}) plot for FPBA SScD.

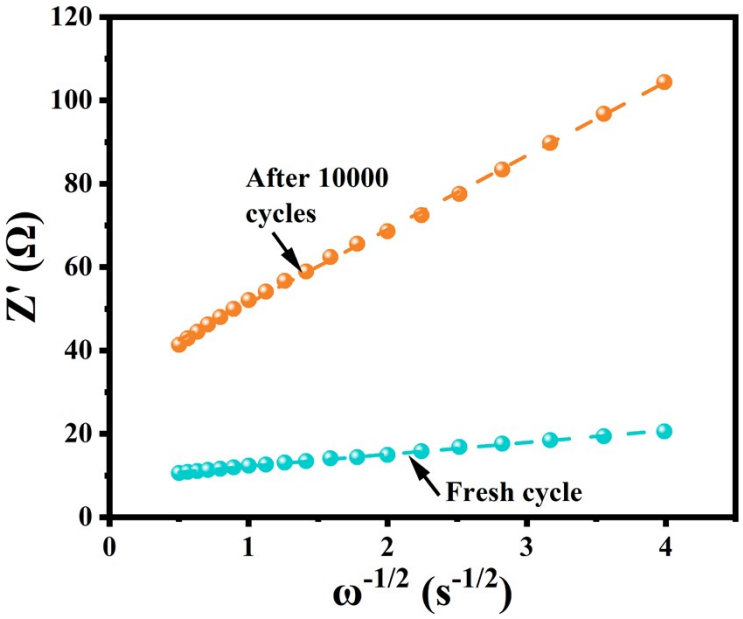

Fig. S16. Kinetics calculation based on the frequency ($\omega^{-1/2}$) and Z′ values of fresh and after 10000 cycles of the FPBA/rGO composite SScD**.**

Table S5. Calculated resistance and diffusion coefficient from EIS spectra of fresh and after 10000 cycles of the FPBA/rGO composite SScD.

	R_S (Ω)	R_{CT} (Ω)	σ (Ω $s^{-1/2}$)	D_{Na+} (cm^2 s^{-1})
Fresh cycle	3.034	5.901	2.861	2.74 □ 10^{-10}
After 10000 cycles	4.041	52.61	17.697	7.16 □ 10^{-12}

Table S6. Comparison table of FPBA/rGO composite SScD.

Electrode material	Operating potential window (V)	Specific capacity (C g^{-1})	Energy density (Wh Kg^{-1})	Power density (W Kg^{-1})	Cyclic retention	Ref.
Graphene@ prussian blue//AC	1.8	44.61 Fg^{-1} (80.29 C g^{-1}) at 0.5 A g^{-1}	20.1	450	87.5% retention at 5 A g^{-1} over 5000 cycles	1
Cobalt hexacyanoferrate//AC	1.4	65.5 Fg^{-1} (91.7 C g^{-1}) at 0.5 A g^{-1}	17.4	1196	91 retentions at 1 A g^{-1} over 6000 cycles	2
Co-Co@Ni-Fe PBA-PPy//AC	1.6	64 Fg^{-1} (102.4 C g^{-1}) at 1 A g^{-1}	20	808.9	79% retention at 10 A g^{-1} over 2000 cycles	3
CoHCF/rGO	2.0	65 Fg^{-1} (130 C g^{-1}) at 1 A g^{-1}	39.6	1000	91% retention at 5 A g^{-1} Over 1000 cycles	4
Ni2CoHCF/NF //AC/NF	1.5	96.9 Fg^{-1} (145.4 C g^{-1}) at 0.5 A g^{-1}	30.59	378.7	94.32 retention at 2 A g^{-1} over 2000 cycles	5
CoHCF//AC	2	78 Fg^{-1} (156 C g^{-1}) at 1 A g^{-1}	42.5	990	89% retention at 5 A g^{-1} over 5000 cycles	6
NiFePBA/rGO/ CC-0.5	2	92 Fg^{-1} (184 C g^{-1}) at 0.5 A g^{-1}	51.11	540	74.38% retention at 5 A g^{-1} over 10000 cycles	7

FPBA/rGO	1.8	138.5 Fg^{-1} (249.3 C g^{-1}) at 1 A g^{-1}	62.32	900	90.5% retention at 10 A g^{-1} over 10000 cycles	**This work**

References:

1 S.-C. Wang, M. Gu, L. Pan, J. Xu, L. Han and F.-Y. Yi, *Dalton Trans.*, 2018, **47**, 13126–13134.

2 Z. Song, W. Liu, Q. Yuan, Q. Zhou, G. Liu and Z. Zhao, *J. Mater. Sci. Mater. Electron.*, 2018, **29**, 14897–14905.

3 P. Mukherjee, V. R. S, A. Borenstein and T. Zidki, *Mater. Chem. Front.*, 2023, **7**, 1110–1119.

4 J.-G. Wang, Z. Zhang, X. Liu and B. Wei, *Electrochimica Acta*, 2017, **235**, 114–121.

5 X. Zhu, H. Tao and M. Li, *Int. J. Hydrog. Energy*, 2020, **45**, 14452–14460.

6 J.-G. Wang, Z. Zhang, X. Zhang, X. Yin, X. Li, X. Liu, F. Kang and B. Wei, *Nano Energy*, 2017, **39**, 647–653.

7 T. Miao, J. Zhang, Y. Wang, K. Fang, Z. Wang, K. Zhan and B. Zhao, *J. Colloid Interface Sci.*, 2023, **648**, 768–777.